IEEE Access
Multidisciplinary | Rapid Review | Open Access Journal

Received July 17, 2021, accepted September 24, 2021, date of publication October 4, 2021, date of current version November 22, 2021.

Digital Object Identifier 10.1109/ACCESS.2021.3117521

First Principal Simulation Study of Human Body Compatible Molecular Single Electron Transistors

MORTEZA BODAGHZADEH[1], MOHAMAD TAGHI AHMADI[1], MAHAN AHMADI[2], SEYED SAEID RAHIMIAN KOLOOR[3], MICHAL PETRŮ[4], AND FATEMEH ESFANDIARI[5]

[1]Nanotechnology Research Center, Nano-Physic Group, Department of Physics, Urmia University, Urmia 57561-51818, Iran
[2]Medical Campus of Xi'an Jiaotong University, Xi'an, Shaanxi 710049, China
[3]Institute for Nanomaterials, Advanced Technologies and Innovation (CXI), Technical University of Liberec (TUL), 461 17 Liberec, Czech Republic
[4]Technical University of Liberec (TUL), 461 17 Liberec, Czech Republic
[5]Faculty of Psychology and Educational Science, Shahid Chamran University of Ahvaz, Ahvaz 61358-13453, Iran

Corresponding authors: Mohamad Taghi Ahmadi (mt.ahmadi@urmia.ac.ir) and Seyed Saeid Rahimian Koloor (s.s.r.koloor@gmail.com)

This work was supported in part by the Ministry of Education, Youth and Sports of the Czech Republic and in part by the European Union (European Structural and Investment Funds-Operational Programme Research, Development, and Education) in the framework of the project "International Research Laboratories," under Grant CZ.02.2.69/0.0/0.0/18_054/0014685.

ABSTRACT Considering the importance of single-electron transistors (SETs), many studies have been done over the past decade to develop the use of SETs and improve their efficiency in both the experimental and theoretical fields. One of the most important challenges in SETs study is their optimization for use in human-compatible Nanobots for purposes such as drug delivery and destruction of cancer cells. Therefore, the use of human-compatible molecules as an island in these transistors is very significant. In this work, the density functional theory (DFT) & non-equilibrium Green's function (NEGF) methods have been used for SETs modeling study of the first principle computations in the coulomb barricade system of SETs based upon the metal-organic complex of ascorbic acid (vitamin C), thiamine (vitamin B1), riboflavin (vitamin B2), nicotinic acid (vitamin B3), pantothenic acid (vitamin B5), pyridoxine (vitamin B6), biotin (vitamin B7) and folic acid (vitamin B9). The isolated molecules and SET structures are analyzed based upon premises of overall energies, ionization energies, affection energies, addition energies, charging energies, gate coupling constant, density of states (DOS) plot, and charge stability diagrams (CSDs). It's established that riboflavin (vitamin B2) in the habitat of SET has a decline in the additional energy and has the lowest addition energy and lowest charging energy at the neutral charge in the SET environment along with higher conductivity as evident from the CSD comparison has been revealed. Summing up the results and analyses indicate that a riboflavin molecule is a suitable option for SETs with a molecular island compatible with the human body.

INDEX TERMS Single-electron transistor (SET), vitamin C, vitamin B group, charging energy, metal-organic complex, charge stability diagram (CSD).

I. INTRODUCTION

Due to the increasing development of electronic equipment and being the incessant scaling down of device sizes, semiconductor devices are very close to their physical limits, there is an instantaneous need to develop next-generation technologies, in the designation of both device structures and physics [1], [2]. With the technology of getting smaller which confronts Moore's law i.e., the transistor poll on a chip multiplies at the rate of 2X per every 2 years [3], so nanoelectronic researchers are greatly keen on studying distinctive nanodevices like carbon nanotube/graphene tunnel field-effect transistors (FETs) and sensors [4]–[8], organic FETs [9], [10], single-molecule devices [11], [12], single-electron transistors (SETs) [13], [14] and junction-less nanowire transistors [15], [16]. For promising features like very fast switching speed and quantum tunneling-based operation, SETs are a substantial topic for researchers [17]. SETs are based on a nano-island such as one molecule sandwiched by tunneling between source and drain electrodes and is coupled with a third electrode (Gate) and at the base of island/quantum dot a single sheet of the dielectric compartment, for controlling the SET that showed in the schematic of Fig. 1 on the island, electrons are limited and quantitative.

The associate editor coordinating the review of this manuscript and approving it for publication was Yee Sin Ang.

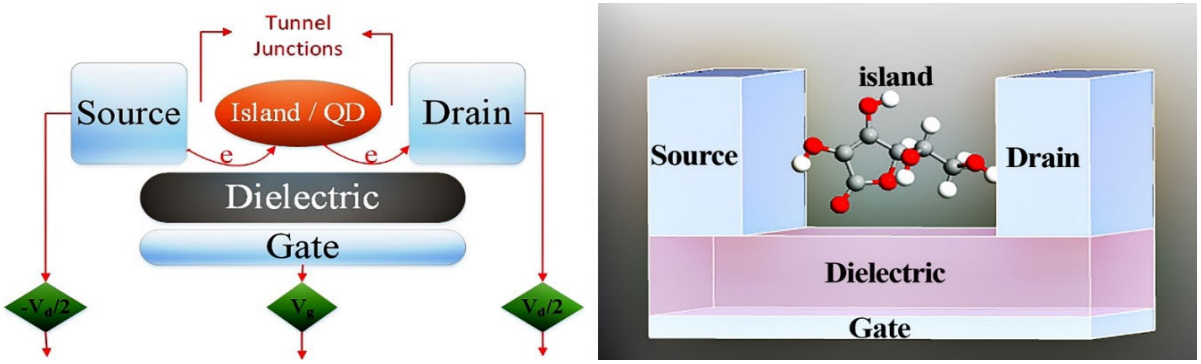

FIGURE 1. The schematic diagram for the single-electron transistor (SET).

The current surplus charges on the SET island. Using quantum dots in SET is because that, addition or removal of a single electron changes the electrostatic energy, and thus inflow and outflow of electrons can be controlled [18], [19].

We can explain the transporting of the electron, by sequential tunneling of single electrons, in SETs. The aforementioned procedure is additionally mentioned as the Coulomb blockade that is the basis for the understanding of molecule-based transistors and affects the energy levels of the island as well as source and drain electrodes [20], [21]. The brief settlement of an electron on the island as a result of no-localization and coherent gesture in the scheme by the burrowed electron from the origin is titled coherent transport (CT), which is the cause of the coherent transport regime (CTR) causing hindrance in the SET when the connectivity amid the island is guarded [22].

Another inhibiting system is the Coulomb blockade (CB) procedure that occurs when a fragile coupling is initiated amidst the electrodes. By the virtue of compensation of the electron on the island to deplete converts into a self-governing from the burrowing procedure of the origin so, for electron transportation, the preference should have the island's electronic level. This supervision of the presence of the electronic level in the preference window is accomplished by the gate electrode. The composed electron burrowing of SET generates ultra-low-power leftovers, as a result of the carrier scattering and inadequacy of impact and bump; so the current intent is to attain Coulomb blockade regime (CBR) for SET [23].

We define the energy of the island with the function of $E^{island}(I)$, and similarly, $E^{source}(S)$ and $E^{drain}(D)$ for the energy of source and drain electrodes [23].

$$E^{source}(S) + E^{island}(I) \geq E^{source}(S-1) + E^{island}(I+1) \quad (1)$$

$$E^{drain}(D) + E^{island}(I+1) \geq E^{drain}(D+1) + E^{island}(I) \quad (2)$$

S, I, and D are the fundamental sum of electrons in the source electrode, island, and drain electrode, correspondingly [24]. The utmost energy of the electron can be shown in the origin electrode with $-W + eV/2$, where V is the enforced bias and W is the work function of the electrode. With tunneling of the electron with the highest energy to the island:

$$E^{source}(S) - E^{source}(S-1) = -W + eV/2 \quad (3)$$

By putting in equation (1) we have:

$$-W + eV/2 + E^{island}(I) \geq E^{island}(I+1) \quad (4)$$

Similarly, $-W + eV/2$ is the minimal energy of an electron in the sewer, and so with equation (3) for drain electrode and equation (2), we have:

$$E^{island}(I+1) \geq -W + eV/2 + E^{island}(I) \quad (5)$$

TABLE 1. Research in various sub-domains of SET technology in the recent years.

Year	Articles
2020	Katkar et al [31]; Khademhosseini et al [32]; Wang et al [33]; Srivastava and Khan [34]; Parashar [35]; Hanurjaya et al [36]; Biswas et al [37]; Tran et al [38]; Bera [39]; Chauhan and Verma [40].
2019	Parekh [41]; Abdelkrim [42]; Patel et al [43]; Khademhosseini et al [44]; Lee et al [45].
2018	Ahsan [46]; KhademHosseini et al [47]; Hosseini et al [21]; Castro et al [48]; Miralaie and Mir [49]; Barraud et al [50]; Bai et al [51]; Patel et al [52].
2017	Delwar et al [53]; Amat et al [54].
2016	Ghosh et al [55]; Willy and Darma [56]; Raut and Dakhole [57]; Miralaie and Mir [58].
2015	Jain et al [59]; Mukherjee et al [60]; Raut and Dakhole [61]; Karbasian et al [62]; Li-Na et al [63].

The necessity for a tide to proceed in the device is:

$$e|V|/2 \geq \Delta E^{island}(I) + W \geq -e|V|/2 \quad (6)$$

where $\Delta E^{island}(I) = E^{island}(N+1) - E^{island}(N)$ is the filling energy of the island [20].

In a SET composition, the sum of organic and inorganic molecules has been certified as an island [25]–[30]. Much valuable research has been done in the field of prospective SET-based technology, and a comprehensive list of this research in recent years has been summarized in Table 1.

One of the important applications of SETs is their use in nanorobots for medical purposes. The dimensions reducing of robots operating system has the potential for advancing medical treatment like accessibility to far-off and difficult parts of the body and execute various medical methods for eliminating tumors and cancer cells. Notwithstanding the development of medical nanorobots in the recent decade, propelling these devices to widespread clinical use is an important necessity and serious challenge of this field that has not been achieved yet. A medical nanorobot is defined as a structure in nano dimensions that consists of a motor that can convert various forms of energy into mechanical force and perform its mission in the body using electrical commands, so the simulating and construction of transistors in molecular and nano dimensions to establish the hardware of these robots is one of the important challenges of this purpose [64]–[69].

Various researches have been done in the field of suitable transistors for these nanorobots [70]–[72] and single-electron transistors with molecular islands compatible with the human body seem to be able to help us achieve this goal because of their unique properties.

In the present study, As the first principal simulation research, vitamins C and B group as organic molecules fully compatible with the human body have been investigated for use in single-electron transistors. The significance of this study is that there are now extensive studies on nanorobots, aimed at drug delivery or the elimination of cancer cells in the body but no study has used organic molecules compatible with the human body, such as vitamins, as the island of single-electron transistors. We need to study single-electron transistors with organic and human-compatible quantum dots, to utilize their nanometer-sized features and high efficiency in nanorobots fabrication in the future. To this end, the use of vitamin C molecules and group B vitamins seems to be appropriate as an island, as they are fully compatible with the needs of the human body and are fully compatible with the cells of the body.

TABLE 2. Basic chemical and physical properties of ascorbic acid (vitamin C), thiamine (vitamin B1), riboflavin (vitamin B2), nicotinic acid (vitamin B3), pantothenic acid (vitamin B5), pyridoxine (vitamin B6), biotin (vitamin B7) and folic acid (vitamin B9) molecules.

	Molecular Formula	Molecular Weight (g/mol)	Topological Polar Surface Area (Å²)
Ascorbic acid	$C_6H_8O_6$	176.12	107
Thiamine	$C_{12}H_{17}N_4OS^+$	300.81	104
Riboflavin	$C_{17}H_{20}N_4O_6$	376.4	155
Nicotinic acid	$C_6H_5NO_2$	123.11	50.2
Pantothenic acid	$C_9H_{17}NO_5$	219.23	107
Pyridoxine	$C_8H_{11}NO_3$	169.18	73.6
Biotin	$C_{10}H_{16}N_2O_3S$	244.31	104
Folic acid	$C_{19}H_{19}N_7O_6$	441.4	209

Source: U.S national center for biotechnology information. PubChem Database. https://pubchem.ncbi.nlm.nih.gov

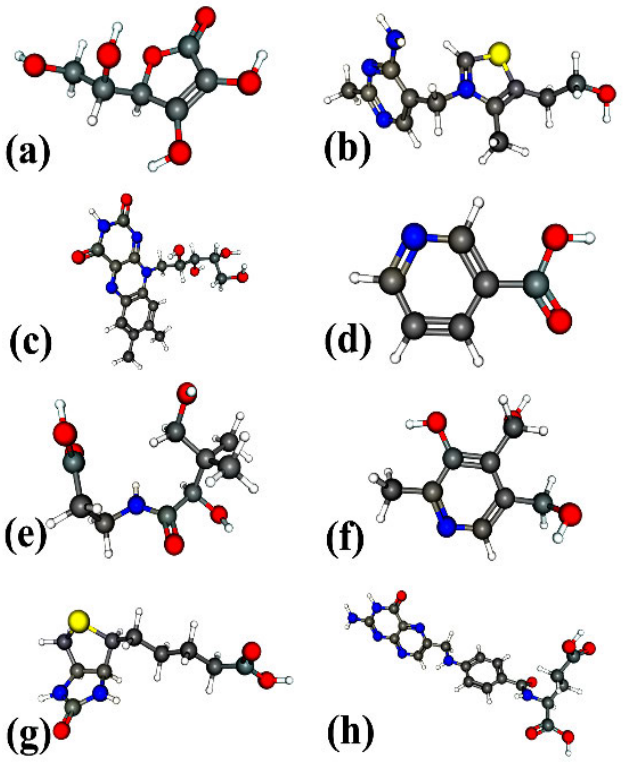

FIGURE 2. Optimized structure of (a) ascorbic acid (vitamin C), (b) thiamine (vitamin B1), (c) riboflavin (vitamin B2), (d) nicotinic acid (vitamin B3), (e) pantothenic acid (vitamin B5), (f) pyridoxine (vitamin B6), (g) biotin (vitamin B7), (h) folic acid (vitamin B9) molecules.

II. METHODS AND COMPUTATIONAL DETAILS

In this work, 8 SETs with ascorbic acid (vitamin C), thiamine (vitamin B1), riboflavin (vitamin B2), nicotinic acid (vitamin B3), pantothenic acid (vitamin B5), pyridoxine (vitamin B6), biotin (vitamin B7) and folic acid (vitamin B9) molecules with chemical and physical properties given in Table 2, like the island, since it can depict organizations with discrete equilibrium and can also replicate molecular & atomic-scale organizations to compute their physical and electrical features; therefore it's modified for which density functional theory (DFT) based Gaussian 03 software and accelerated utilizing the Atomistix Toolkit-Virtual Nano Lab (ATK-VNL) software seeing that it consists of a collection of atomic-scale modeling methods.

The optimized structure of ascorbic acid (vitamin C), thiamine (vitamin B1), riboflavin (vitamin B2), nicotinic acid (vitamin B3), pantothenic acid (vitamin B5), pyridoxine (vitamin B6), biotin (vitamin B7), and folic acid (vitamin B9) are shown in Fig. 2.

III. RESULTS AND DISCUSSION

Based upon academic and exploratory studies and researches, there are 2 procedures recommended primarily which are adaptable with the inspections on interface coupling amid molecules and electrodes. The first procedure which alters

all molecular orbitals likewise whereas relocating them in an identical route (up or down), accommodates the interfacial dipole which is developed due to fractional charge conversion amid the orbitals of the molecule and electrode. The second procedure is renormalization of the transported gap, in which figure charges in the electrodes due to the motion of electrons are the base of this happening (either added or removed from the molecules), by which in this method the involved degrees migrate upwards and the disengaged ones migrate downwards energy-wise.

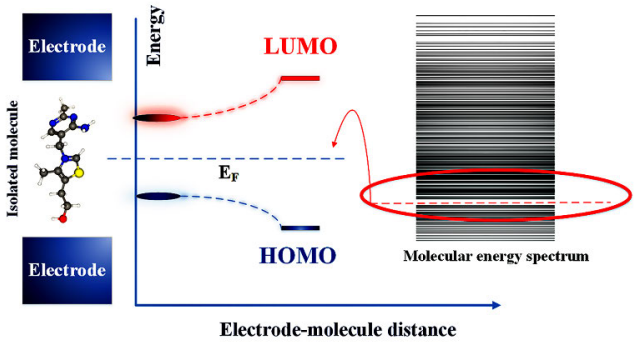

FIGURE 3. The schematic diagram for the HOMO-LUMO gap.

In the two procedures, the diversion in molecular energy levels is positively correlated with the cohesion of the interface coupling. We need to comprehend the disparity among the highest occupied molecular orbital (HOMO) and lowest unoccupied molecular orbital (LUMO), to define the classification of orbital energy grades and transport gap structure revision with the electrode mass of conditions expands at the Fermi level. HOMO is investigated as the minimum of the valence band and LUMO is considered the maximum of the conduction band. These two parameters have extensive momentous during the investigation of the analytical design of nanoscale devices. The gap betwixt HOMO and LUMO expresses the thermodynamic stability of the molecular device. The higher gap is the higher stability. The alterations of HOMO-LUMO gaps happen because of the changes in energy levels, indeed the changes of HOMO and LUMO energy levels [73] that are shown in Fig. 3. It should be noted that semi-local DFT methods can underestimate HOMO-LUMO energy gaps which can affect NEGF transport [74], [75].

DFT calculations for all energy levels of each natural molecules of ascorbic acid (vitamin C), thiamine (vitamin B1), riboflavin (vitamin B2), nicotinic acid (vitamin B3), pantothenic acid (vitamin B5), pyridoxine (vitamin B6), biotin (vitamin B7) and folic acid (vitamin B9) molecules were performed by ATK software. From software output data, the respective E_{HOMO}, and E_{LUMO} are reported in Table 3.

The HOMO-LUMO division is discovered to be 3.37 eV, 3.51 eV, 2.01 eV, 3.18 eV, 4.38 eV, 3.89 eV, 3.8 eV, and 1.83 eV for ascorbic acid (vitamin C), thiamine (vitamin B1), riboflavin (vitamin B2), nicotinic acid (vitamin B3), pantothenic acid (vitamin B5), pyridoxine (vitamin B6), biotin (vitamin B7) and folic acid (vitamin B9) molecules, respectively. The merest amount in the HOMO-LUMO diversion is detected for folic acid (vitamin B9) and riboflavin (vitamin B2) molecules because the lower HOMO-LUMO gap refers to higher conductivity of the molecule [76].

In the following, the simulation of SET in the electrostatic environment is accomplished by utilizing ATK-VNL with designing which is shown in Fig. 4. For the geometry of SET, we used a 3.7-angstrom wide dielectric strip with a dielectric constant of 10 ε_0, and a metal back-gate with 1-angstrom thickness, and encircled by origin and culvert metal electrodes with 4-angstrom thickness. The electrodes were selected from gold with a work function equal to W = 5.28 eV and amidst the origin-culvert electrodes, the molecules are situated on the gate electrode which is garnished with the gate dielectric. All the 8 molecules are designed in the SET composition utilizing DFT established ATK-VNL program with double-zeta polarized (DZP) and local density approximation (LDA) based appointed for broadening the wave tasks. The Poisson solve scheme has been brought to use with Neumann boundary circumstances so that we can have zero units of the common electric terrain at the borders.

Overall energies have been forecasted so that we can dissect the charge cohesion diagram for the particular SETs, as the SETs have been accelerating for the islands/molecules. Total energies for distinct charge states -2, -1, 0, $+1$, $+2$ for the simulated structures, and the sum of energy was computed for various charge cases of the SETs which are disclosed in Table 3. To acquire the charging energies the ground-state total energies of the neutral island/molecule in the SET environment for ascorbic acid (vitamin C), thiamine (vitamin B1), riboflavin (vitamin B2), nicotinic acid (vitamin B3), pantothenic acid (vitamin B5), pyridoxine (vitamin B6), biotin (vitamin B7) and folic acid (vitamin B9) are calculated to be -3676.45 eV, -4035.10 eV, -6686.69 eV, -2163.38 eV, -4131.11 eV, -3007.82 eV, -4033.76 eV and -7800.22 eV, respectively. It can be seen that folic acid (vitamin B9) and riboflavin (vitamin B2) have the lowest ground state total energies and therefore they're more balanced compared to the other 6 molecules.

The energy that needs to include an electron to the island is affinity energy (EA) and the energy needed to charge the funnel intersection with one main charge designated as the charging energy also ionization energy (EI) is the energy needed to eradicate an electron from the island:

$$E_I = E(N-1)\,E(N) = E^{+1}\,E^0 \tag{7}$$

$$E_A = E(N+1)E(N) = E^{-1}E^0 \tag{8}$$

where E(N) or E^0 is the overall energy of the impartial system having N electrons, E(N − 1) or E^{+1} is the overall energy of the positively charged system having N1 electron, and E(N + 1) or E^{-1} is the overall energy of the negatively charged system having N + 1 electrons [77].

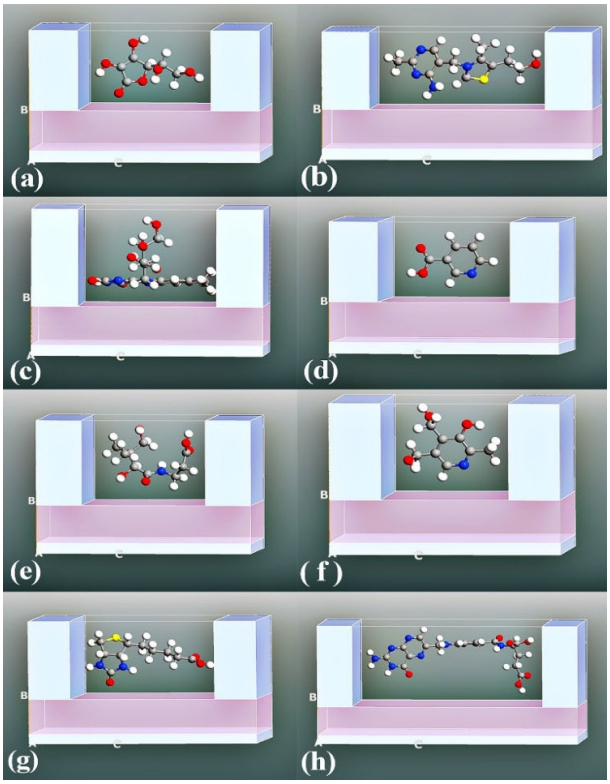

FIGURE 4. The SET configuration of (a) ascorbic acid (vitamin C), (b) thiamine (vitamin B1), (c) riboflavin (vitamin B2), (d) nicotinic acid (vitamin B3), (e) pantothenic acid (vitamin B5), (f) pyridoxine (vitamin B6), (g) biotin (vitamin B7), (h) folic acid (vitamin B9).

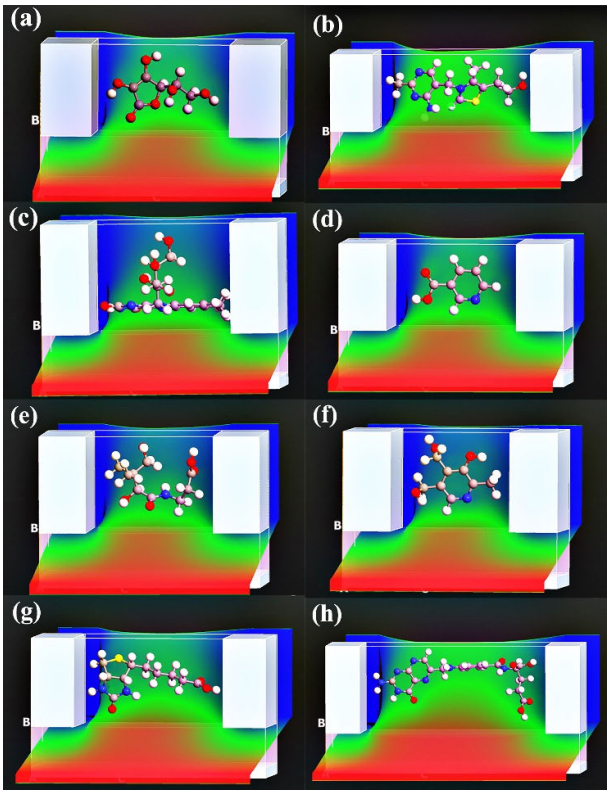

FIGURE 5. The contour plot shows the induced electrostatic potential for SET configuration of (a) ascorbic acid (vitamin C), (b) thiamine (vitamin B1), (c) riboflavin (vitamin B2), (d) nicotinic acid (vitamin B3), (e) pantothenic acid (vitamin B5), (f) pyridoxine (vitamin B6), (g) biotin (vitamin B7), (h) folic acid (vitamin B9).

Correspondingly, for the consecutive molecular system, ionization and affinity energy are:

$$E_I^{+1} = E^{+2}\,E^{+1} \tag{9}$$

$$E_A^{-1} = E^{-2}E^{-1} \tag{10}$$

and also, additional energy (Eadd) is the contrast amidst ionization energy and affinity energy and is shown as [78]:

$$E_{add} = E_A E_I \tag{11}$$

TABLE 3. E_{Total} for states 0, +1, −1, +2, −2, highest energy occupied molecular orbital (E_{HOMO}), lowest energy unoccupied molecular orbital (E_{HOMO}), ionization energies (E_I and E_I^{+1}), affinity energies (E_A and E_A^{-1}) and additional energy (E_{add}) of ascorbic acid (vitamin C), thiamine (vitamin B1), riboflavin (vitamin B2), nicotinic acid (vitamin B3), pantothenic acid (vitamin B5), pyridoxine (vitamin B6), biotin (vitamin B7) and folic acid (vitamin B9) in the isolated environment and the SET environment.

	Energy(eV)	Vitamin C	Vitamin B1	Vitamin B2	Vitamin B3	Vitamin B5	Vitamin B6	Vitamin B7	Vitamin B9
Isolated environment	E^{+2}	- 3659.85	- 4025.90	- 6673.50	- 2146.69	- 4116.53	- 2993.51	- 4002.04	- 7788.24
	E^{+1}	- 3670.18	- 4032.80	- 6680.81	- 2156.37	- 4124.82	- 3001.62	- 4025.90	- 7794.96
	E^{0}	- 3676.51	- 4035.30	- 6686.84	- 2163.44	- 4131.35	- 3007.93	- 4033.73	- 7800.46
	E^{-1}	- 3676.41	- 4035.69	- 6689.12	- 2164.86	- 4131.23	- 3008.44	- 4030.76	- 7802.01
	E^{-2}	- 3674.36	- 4034.44	- 6689.39	- 2164.11	- 4129.55	- 3007.11	- 4030.63	- 7802.35
	E_{LUMO}	- 1.30	- 1.31	- 3.27	- 2.46	- 1.12	- 1.54	- 0.79	- 2.70
	E_{HOMO}	- 5.03	- 4.82	- 5.28	- 5.64	- 5.50	- 5.43	- 4.59	- 4.53
	E_I^{+1}	10.33	6.9	7.31	9.68	8.29	8.11	23.86	6.72
	E_I	6.33	2.5	6.03	7.07	6.53	6.31	7.83	5.5
	E_A	0.1	- 0.39	- 2.28	- 1.42	0.12	- 0.51	2.97	- 1.55
	E_A^{-1}	2.05	1.25	- 0.27	0.75	1.68	1.33	0.13	- 0.34
	E_{add}	- 6.23	- 2.89	- 8.31	- 8.49	- 6.41	- 6.82	- 4.86	- 7.05
SET environment	E^{+2}	- 3659.26	- 4023.99	- 6672.36	- 2143.39	- 4114.15	- 2988.78	- 4017.95	- 7780.46
	E^{+1}	- 3669.50	- 4032.28	- 6680.48	- 2155.59	- 4124.12	- 3001.10	- 4027.48	- 7794.30
	E^{0}	- 3676.45	- 4035.10	- 6686.69	- 2163.38	- 4131.11	- 3007.82	- 4033.76	- 7800.22
	E^{-1}	- 3675.95	- 4034.67	- 6688.92	- 2163.78	- 4130.37	- 3007.47	- 4032.42	- 7800.53
	E^{-2}	- 3672.45	- 4031.67	- 6689.12	- 2160.23	- 4126.93	- 3004.06	- 4011.09	- 7798.26
	E_I^{+1}	10.24	8.29	8.12	12.2	9.97	12.32	9.53	13.84
	E_I	6.95	2.82	6.21	7.79	6.99	6.72	6.28	5.92
	E_A	0.5	0.43	- 2.23	- 0.4	0.74	0.35	1.34	- 0.31
	E_A^{-1}	3.5	3	- 0.2	3.55	3.44	3.41	21.33	2.27
	E_{add}	- 6.45	- 2.39	- 8.44	- 8.19	- 6.25	- 6.37	- 4.94	- 6.23

TABLE 4. Charging energies, $E^{n-1} - E^{n}$ of different charge states of ascorbic acid (vitamin C), thiamine (vitamin B1), riboflavin (vitamin B2), nicotinic acid (vitamin B3), pantothenic acid (vitamin B5), pyridoxine (vitamin B6), biotin (vitamin B7), and folic acid (vitamin B9) in the isolated and SET environment at zero gate voltage.

	Charging Energy(eV)	Vitamin C	Vitamin B1	Vitamin B2	Vitamin B3	Vitamin B5	Vitamin B6	Vitamin B7	Vitamin B9
Isolated	+2	- 10.33	- 6.91	- 7.31	- 9.67	- 8.29	- 8.10	- 23.86	- 6.72
	+1	- 6.33	- 2.49	- 6.03	- 7.07	- 6.54	- 6.31	- 7.83	- 5.51
	0	0.10	- 0.39	- 2.28	- 1.42	0.13	- 0.51	2.98	- 1.55
	-1	2.05	1.25	- 0.27	0.75	1.68	1.34	0.13	- 0.34
SET	+2	- 10.24	- 8.29	- 8.12	- 12.20	- 9.97	- 12.32	- 9.53	- 13.84
	+1	- 6.94	- 2.82	- 6.21	- 7.79	- 6.99	- 6.72	-6.28	- 5.92
	0	0.50	0.42	- 2.24	- 0.40	0.74	0.35	1.34	- 0.31
	-1	3.51	3.01	- 0.20	3.55	3.44	3.41	21.33	2.27

Ionization energies, affinity energies, and additional energy for both the segregated habitat and the SET habitat are reported in Table 3. It can be seen in Table 3 that, riboflavin (vitamin B2) has decremented in the additional energy and has the lowest addition energy and from Table 4, it can be seen that it has the lowest charging energy at the neutral charge in a SET environment, resulting in an enhanced balance of the molecule and transforming into an improved selection for brisk transmission is a SET habitat. In Table 4, the charging energies computed for all the molecules are reported for isolated and SET configuration at zero gate voltage. Stabilization of charge on the molecules by the electrostatic neighboring in a SET habitat is the reason for the devaluation in $+2$ and $+1$ charge conditions of charging energies that can be seen in most circumstances from detached to SET habitat to the molecules in Table 4.

The alteration of overall energies with relevance to gate voltage for various charge conditions is demonstrated in Fig. 6 in which various charge conditions are given differing colors, blue for -2, green for -1, red for 0, turquoise for 1, and violet for 2. To analyze the overall energies of various charge conditions, it's considerable to include the energy of the supplementary electron. The energy of a supplementary electron is given by the work function of the golden electrode as an electron cache. The balanced charge condition of the molecules for a given gate voltage is the minimum energy condition.

From the positive gate, the molecule ingests an electron transforming it negatively charged and fluctuating the LUMO level of the molecule to below the electrode's Fermi level, which leads to the cohesion examination. Rejecting an electron at the negative gate molecule, transforming it positively charged and the HOMO level of the molecule transforms to be exposed beyond the electrode's Fermi level. The indifferent condition is the minimum energy condition, in the field surrounding zero gate voltage, since the gate calamity is nearly linear and the tilt is linked to the charge condition of the molecule.

As can be seen in Fig. 6, all the molecules are at their minimal energy form in their indifferent condition in 0 charge condition (red) and thus are more balanced in their indifferent condition. Gate coupling constant (α) for ascorbic acid (vitamin C), thiamine (vitamin B1), riboflavin (vitamin B2), nicotinic acid (vitamin B3), pantothenic acid (vitamin B5), pyridoxine (vitamin B6), biotin (vitamin B7) and folic acid (vitamin B9) SETs are reported in Table 5. To attainment as many charge states as possible, the gate coupling constant must be large enough. Therefore, the gate coupling constant for folic acid (vitamin B9), thiamine (vitamin B1), and riboflavin (vitamin B2) calculated 0.45, 0.44, and 0.38 which were more coupled with gate than other molecules and these are in a better state than other SETs, respectively and show an almost linear relationship among the total energy and the gate potential than others, since all atoms are approximately shifted by the gate potential identically, as can be seen in Fig. 5 that has obtained electrostatic potential induced by the gate voltage for all SETs by subtracting the potential (at zero gate voltage) from the electrostatic potential (at a given gate voltage).

The density of states (DOS) plot evinced as a function of energy demonstrates the numeral of states that exist in a structure per unit of energy and is necessary for ascertaining the energy dispensations of carriers and carrier concentrations. This evaluation should also be performed to give a better understanding of charge flow due to variation at the molecular level due to applied gate voltage. especially, to justify the

TABLE 5. Gate coupling constant (α) for ascorbic acid (vitamin C), thiamine (vitamin B1), riboflavin (vitamin B2), nicotinic acid (vitamin B3), pantothenic acid (vitamin B5), pyridoxine (vitamin B6), biotin (vitamin B7) and folic acid (vitamin B9) SETs.

	Charge state	Vitamin C	Vitamin B1	Vitamin B2	Vitamin B3	Vitamin B5	Vitamin B6	Vitamin B7	Vitamin B9
Gate coupling constant	+2	0.6152	0.9503	0.7433	0.6796	0.5492	0.4649	0.5388	1.0288
	+1	0.2720	0.5605	0.3856	0.3297	0.2642	0.2296	0.2129	0.3423
	0	-0.0499	0.0635	0.0204	-0.0266	-0.0313	-0.0116	-0.1048	-0.0583
	-1	-0.4107	-0.3944	-0.3858	-0.3659	-0.3106	-0.2610	-0.4137	-0.4415
	-2	-0.7223	-0.7828	-0.7865	-0.7053	-0.5890	-0.5011	-0.5278	-0.8077
Gate coupling divided by charge state		0.3358	0.4421	0.3831	0.3465	0.2851	0.2423	0.2760	0.4457

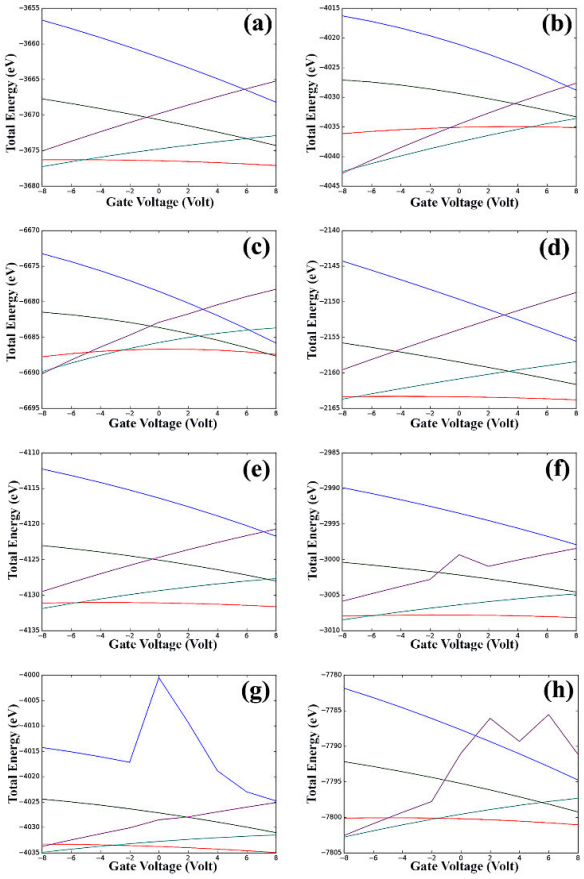

FIGURE 6. The total energy as a function of the gate voltage for (a) ascorbic acid (vitamin C), (b) thiamine (vitamin B1), (c) riboflavin (vitamin B2), (d) nicotinic acid (vitamin B3), (e) pantothenic acid (vitamin B5), (f) pyridoxine (vitamin B6), (g) biotin (vitamin B7), (h) folic acid (vitamin B9) SETs. Different curves are for different charge states of the SET, blue (-2), green (-1), red (0), turquoise (1), and violet (2).

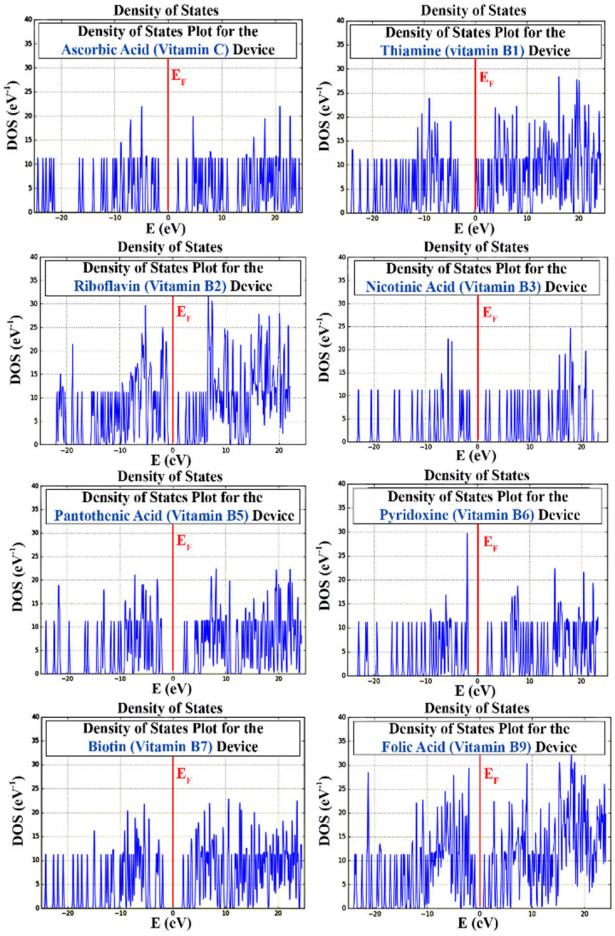

FIGURE 7. Density of states (DOS) plots for the SET configuration of ascorbic acid (vitamin C), thiamine (vitamin B1), riboflavin (vitamin B2), nicotinic acid (vitamin B3), pantothenic acid (vitamin B5), pyridoxine (vitamin B6), biotin (vitamin B7) and folic acid (vitamin B9) molecules.

shift in energy levels due to applied gate voltage [79]. For this purpose, state density diagrams were calculated and plotted for each of the 8 devices, which are shown comparatively in Fig. 7. In the magnified view of Fig. 7, it can be seen that the DOS plot for the SET configuration of riboflavin (vitamin B2) and folic acid (vitamin B9), were significantly different from all other DOS curves, and these two devices have many abrupt spikes in energy states and sharp energy peaks in their DOS plot. These sharper energy peaks show the more conductivity of these SET devices [80].

The applicability among the overall energy and the gate capability for the other 6 molecules is nonlinear. For these molecules, the gate coupling evolves into a tinier form, considering that the atoms nearest to the dielectric domain evaluate the gate capacity for the remainder of the molecule. Polarization energy that grants the second-order addition to the overall energy, because the charges on the various atoms in the molecule permit the formation of a molecular dipole. Charge stability diagrams (CSD) have been devised to examine the transmission by computing the sum of energies of different charge conditions of the molecules as a behavior of gate voltage and the origin-culvert tendency for all molecules of the vitamin C and vitamin B group considered and are conferred in Fig. 8 and for SETs expressed in Fig. 9. Contrasting shades indicate the number of molecular grades existing inside the tendency window (dark blue as 0 energy level, light blue as 1 energy level, turquoise as 2 energy levels, yellow as 3 energy levels, and red as 4 energy levels). CSDs are surveyed for all the molecules to examine the transmission and conversion pace of their molecular and specific SET composition. Source-drain bias, gate voltage, and central diamond area, extracted from charge stability diagrams (CSDs) for molecular and respective SET configurations are reported in Table 6.

In consonance with Table 6 and results from analysis of CSDs of all the islands in Fig. 9, it's discovered that the gate voltage difference (ΔV_g) of the molecules in the SET surrounding is deteriorating and thus the excitement energy required to deliver the SET within an initiation condition is declining according to the arrangement of biotin (7.74 V) > pantothenic acid (7.73 V) > nicotinic acid (7.46 V) > ascorbic acid (7.4 V) > pyridoxine (7.07 V) > folic acid (5.6 V) > riboflavin (3.99 V) > thiamine(3.33 V). By calculating the area of the central diamond for all

TABLE 6. Source-drain bias, gate voltage, and central diamond area, extracted from charge stability diagrams (CSDs) for molecular and respective SET configurations of ascorbic acid (vitamin C), thiamine (vitamin B1), riboflavin (vitamin B2), nicotinic acid (vitamin B3), pantothenic acid (vitamin B5), pyridoxine (vitamin B6), biotin (vitamin B7) and folic acid (vitamin B9).

		Min V_{ds}, Max V_{ds} (Volt)	ΔV_{ds} (Volt)	Min V_g, Max V_g (Volt)	ΔV_g (Volt)	Central Diamond Area
Ascorbic acid (Vitamin C)	Isolated	-6.29, 6.29	12.58	-5.40, 1.00	6.4	40.27
	SET	-7.30, 7.30	14.6	-5.80, 1.60	7.4	54.01
Thiamine (Vitamin B1)	Isolated	-2.07, 2.07	4.14	-4.93, -2.80	2.13	4.42
	SET	-3.13, 3.13	6.26	-5.73, -2.40	3.33	10.45
Riboflavin (Vitamin B2)	Isolated	-3.67, 3.67	7.34	-3.07, 0.80	3.87	14.20
	SET	-3.90, 3.90	7.8	-3.06, 0.93	3.99	15.60
Nicotinic acid (Vitamin B3)	Isolated	-5.53, 5.53	11.06	-3.87, 1.73	5.6	30.98
	SET	-7.37, 7.37	14.74	-4.93, 2.53	7.46	54.98
Pantothenic acid (vitamin B5)	Isolated	-6.60, 6.60	13.2	-5.47, 1.20	6.67	44.01
	SET	-7.67, 7.67	15.34	-6.00, 1.73	7.73	59.30
Pyridoxine (Vitamin B6)	Isolated	-5.77, 5.77	11.54	-4.80, 1.07	5.87	33.83
	SET	-7.00, 7.00	14	-5.60, 1.47	7.07	49.47
Biotin (Vitamin B7)	Isolated	-7.92, 7.92	15.84	-5.47, 2.53	8	63.36
	SET	-7.63, 7.63	15.26	-6.67, 1.07	7.74	58.98
Folic acid (Vitamin B9)	Isolated	-3.90, 3.90	7.8	-3.73, 0.27	4	15.60
	SET	-5.53, 5.53	11.06	-4.93, 0.67	5.6	30.99

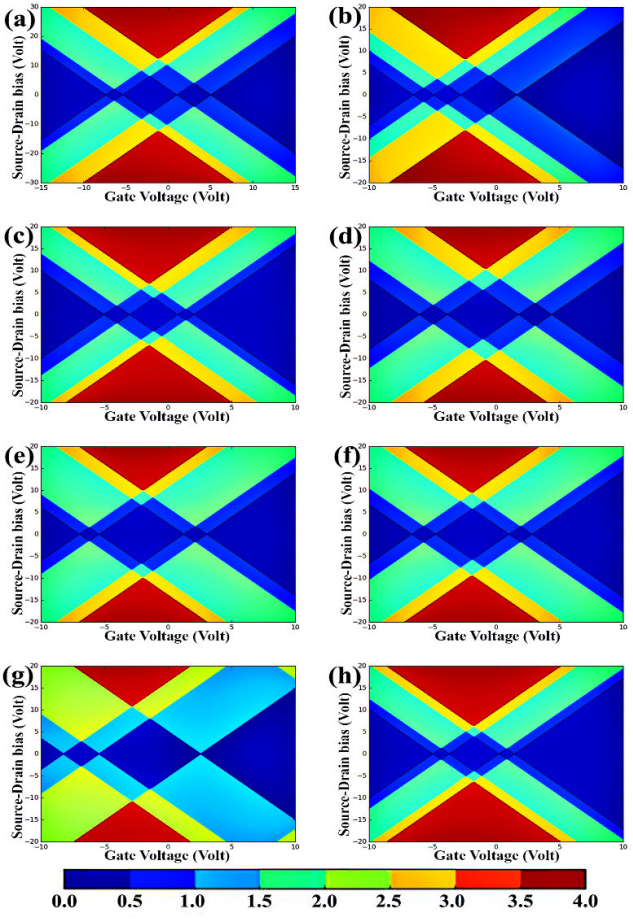

FIGURE 8. The charge stability diagram plots for (a) vitamin C, (b) vitamin B1, (c) vitamin B2, (d) vitamin B3, (e) vitamin B5, (f) vitamin B6, (g) vitamin B7, (h) vitamin B9, isolated molecules. The colors show the number of charge states in the bias win.

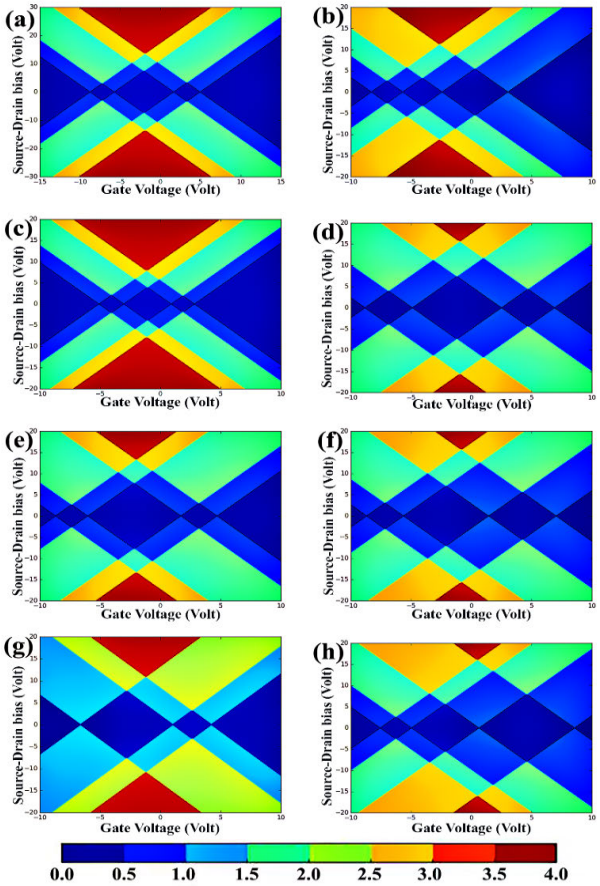

FIGURE 9. The charge stability diagram plots for the SET configuration of (a) vitamin C, (b) vitamin B1, (c) vitamin B2, (d) vitamin B3, (e) vitamin B5, (f) vitamin B6, (g) vitamin B7, (h) vitamin B9 molecules. The colors show the number of charge states in the bias window for a given gate voltage. The color map is blue (0), light blue (1), green (2), orange (3), and red (4) As shown in the diagrams below.

designed SETs, we conclude that the same expression is seen again. Thiamine (vitamin B1), riboflavin (vitamin B2), and folic acid (vitamin B9) have the least central diamond areas in the charge stability diagrams (CSDs), respectively.

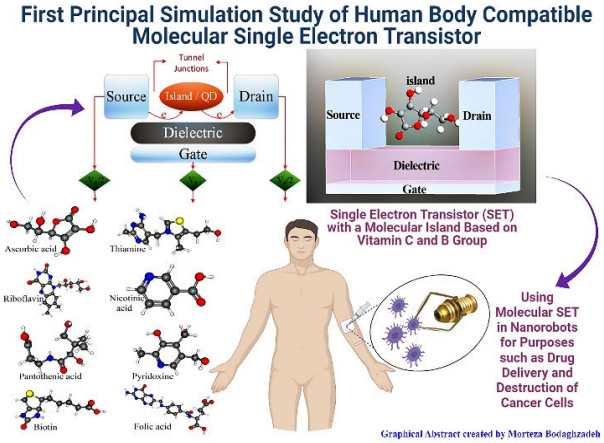

FIGURE 10. Graphical abstract.

Taking into account all the investigations carried out in this study, the molecule riboflavin (vitamin B2) in the SET habitat demonstrates a decline in the supplementary energy and has the minimum amount of extensional energy and lowest charging energy at the neutral charge in the SET environment, thus finding an enhanced transitive and conductive island compared to the other molecules of vitamin C and B group. Besides, CSDs aid it for the improved island operations which their basis is SET.

IV. CONCLUSION

Nowadays making nanometer-sized transistors compatible with the human body, for use in nanorobots built for missions such as drug delivery or to destroy cancer cells absorbed more attention. In this research, the single-electron transistor utilizing ascorbic acid (vitamin C), thiamine (vitamin B1), riboflavin (vitamin B2), nicotinic acid (vitamin B3), pantothenic acid (vitamin B5), pyridoxine (vitamin B6), biotin (vitamin B7) and folic acid (vitamin B9) as the island was investigated. Via utilizing the bundle of Gaussian 03 and ATK-VNL by exploiting DFT and NEGFS techniques these SETs have been accelerated. An analysis of accelerated SETs, overall energies, extension and charging energies, ionization and resemblance energies, density of states (DOS) plot, and charge stability diagrams (CSDs) have been done, to fathom their demeanor and efficiency. At the zero-gate voltage, they are balanced while they're in their indifferent condition since their overall energy vs. gate voltage design demonstrates the same at all of the islands. Gate coupling constant for folic acid (vitamin B9), thiamine (vitamin B1), and riboflavin (vitamin B2) calculated 0.45, 0.44, and 0.38 which were more coupled with gate than other molecules respectively. The analysis of the CSD comparison shows that riboflavin (vitamin B2) in the SET environment represents a reduction in the additional energy and has the lowest additional energy and lowest charging energy at the neutral charge in the SET environment along with higher conductivity. In both cases, the isolated molecule and the SET environment, charge stability diagrams (CSDs) shows that thiamine (vitamin B1), riboflavin (vitamin B2), and folic acid (vitamin B9) have the least central diamond areas respectively, therefore, they have a higher electron transfer rate and better performance than other molecules in the SET environment. Summing up the results and analyses indicate that a riboflavin molecule is a suitable option for a single-electron transistor with a molecular island compatible with the human body.

APPENDIX

See Figure 10.

REFERENCES

[1] L. Cao, F. Altomare, H. Guo, M. Feng, and A. M. Chang, "Coulomb blockade correlations in a coupled single-electron device system," *Solid State Commun.*, vol. 296, pp. 12–16, Jul. 2019, doi: 10.1016/j.ssc.2019.04.004.
[2] M. M. Waldrop, "The chips are down for Moore's law," *Nature*, vol. 530, no. 7589, p. 144, 2016, doi: 10.1038/530144a.
[3] R. R. Schaller, "Moore's law: Past, present, and future," *IEEE Spectr.*, vol. 34, no. 6, pp. 52–59, Jun. 1997, doi: 10.1109/6.591665.
[4] F. Obite, G. Ijeomah, and J. S. Bassi, "Carbon nanotube field effect transistors: Toward future nanoscale electronics," *Int. J. Comput. Appl.*, vol. 41, no. 2, pp. 149–164, Mar. 2019, doi: 10.1080/1206212X.2017.1415111.
[5] E. Penzo, M. Palma, D. A. Chenet, G. Ao, M. Zheng, J. C. Hone, and S. J. Wind, "Directed assembly of single wall carbon nanotube field effect transistors," *ACS Nano*, vol. 10, no. 2, pp. 2975–2981, Feb. 2016, doi: 10.1021/acsnano.6b00353.
[6] L. Britnell, R. V. Gorbachev, R. Jalil, B. D. Belle, F. Schedin, A. Mishchenko, T. Georgiou, M. I. Katsnelson, L. Eaves, S. V. Morozov, and N. M. R. Peres, "Field-effect tunneling transistor based on vertical graphene heterostructures," *Science*, vol. 335, no. 6071, pp. 947–950, Feb. 2012, doi: 10.1126/science.1218461.
[7] S. Suzuki, A. M. M. Hammam, M. E. Schmidt, M. Muruganathan, and H. Mizuta, "Scaling effect on device performance in graphene tunnel field effect transitors," in *Proc. IEEE 18th Int. Conf. Nanotechnol. (IEEE-NANO)*, Jul. 2018, pp. 1–4, doi: 10.1109/NANO.2018.8626305.
[8] M. T. Ahmadi, M. Bodaghzadeh, S. S. R. Koloor, and M. Petrů, "Graphene nanoparticle-based, nitrate ion sensor characteristics," *Nanomaterials*, vol. 11, no. 1, p. 150, Jan. 2021, doi: 10.3390/nano11010150.
[9] H.-J. Kwon, H. Ye, T. K. An, J. Hong, C. E. Park, Y. Choi, S. Shin, J. Lee, S. H. Kim, and X. Li, "Highly stable flexible organic field-effect transistors with Parylene-C gate dielectrics on a flexible substrate," *Organic Electron.*, vol. 75, Dec. 2019, Art. no. 105391, doi: 10.1016/j.orgel.2019.105391.
[10] F. A. Larik, M. Faisal, A. Saeed, Q. Abbas, M. A. Kazi, N. Abbas, A. A. Thebo, D. M. Khan, and P. A. Channar, "Thiophene-based molecular and polymeric semiconductors for organic field effect transistors and organic thin film transistors," *J. Mater. Sci., Mater. Electron.*, vol. 29, no. 21, pp. 17975–18010, Aug. 2018, doi: 10.1007/s10854-018-9936-9.
[11] D. Vuillaume, "Molecular electronics: From single-molecule to large-area devices," 2019, *arXiv:1905.05346*. [Online]. Available: http://arxiv.org/abs/1905.05346
[12] S. Richter, E. Mentovich, and R. Elnathan, "Realization of molecular-based transistors," *Adv. Mater.*, vol. 30, no. 41, Jun. 2018, Art. no. 1706941, doi: 10.1002/adma.201706941.
[13] K. Stokbro, "First-principles modeling of molecular single-electron transistors," *J. Phys. Chem. C*, vol. 114, no. 48, pp. 20461–20465, Jul. 2010, doi: 10.1021/jp104811r.
[14] A. Agarwal, P. C. Pradhan, and B. P. Swain, "From FET to SET: A review," in *Advances in Electronics, Communication and Computing* (Lecture Notes in Electrical Engineering), vol. 443, A. Kalam, S. Das, and K. Sharma, Eds. Singapore: Springer, Oct. 2018, pp. 199–209, doi: 10.1007/978-981-10-4765-7_21.
[15] M. A. Pavanello, R. Trevisoli, R. T. Doria, and M. de Souza, "Static and dynamic compact analytical model for junctionless nanowire transistors," *J. Phys., Condens. Matter*, vol. 30, no. 33, Jul. 2018, Art. no. 334002, doi: 10.1088/1361-648X/aad34f.
[16] H. Lou, L. Zhang, Y. Zhu, X. Lin, S. Yang, J. He, and M. Chan, "A junctionless nanowire transistor with a dual-material gate," *IEEE Trans. Electron Devices*, vol. 59, no. 7, pp. 1829–1836, Jul. 2012, doi: 10.1109/TED.2012.2192499.

[17] V. Milo, G. Malavena, C. M. Compagnoni, and D. Ielmini, "Memristive and CMOS devices for neuromorphic computing," *Materials*, vol. 13, no. 1, p. 166, Jan. 2020, doi: 10.3390/ma13010166.

[18] A. Deyasi and A. Sarkar, "Effect of temperature on electrical characteristics of single electron transistor," *Microsyst. Technol.*, vol. 25, no. 5, pp. 1875–1880, May 2019, doi: 10.1007/s00542-018-3725-5.

[19] M. Kozłowski and J. Marciak-Kozłowska. (2012). *Cancer Tumor Life: Biological & Physical Aspects. Nova Science*. [Online]. Available: https://www.researchgate.net/profile/Miroslaw_Kozlowski5/publication/299499492_Cancer_tumor_life/links/56fbf40f08aef6d10d91b743/Cancer-tumor-life

[20] J. J. Henderson, C. M. Ramsey, E. Del Barco, A. Mishra, and G. Christou, "Fabrication of nanogapped single-electron transistors for transport studies of individual single-molecule magnets," *J. Appl. Phys.*, vol. 101, no. 9, Apr. 2007, Art. no. 09E102, doi: 10.1063/1.2671613.

[21] V. K. Hosseini, M. T. Ahmadi, S. Afrang, and R. Ismail, "Analysis and simulation of Coulomb blockade and Coulomb diamonds in fullerene single electron transistors," *J. Nanoelectron. Optoelectron.*, vol. 13, no. 1, pp. 138–143, Jan. 2018, doi: 10.1166/jno.2018.2211.

[22] A. Srivastava and M. S. Khan, "Charge stability diagram and addition energy spectrum for single-electron transistor based on Ni-dithiolene derivatives," *Organic Electron.*, vol. 59, pp. 125–130, Aug. 2018, doi: 10.1016/j.orgel.2018.05.003.

[23] S. Shityakov, N. Roewer, C. Förster, and J.-A. Broscheit, "In silico modeling of Indigo and Tyrian purple single-electron nano-transistors using density functional theory approach," *Nanosc. Res. Lett.*, vol. 12, no. 1, pp. 1–8, Jul. 2017, doi: 10.1186/s11671-017-2193-7.

[24] E.-H. Lee and K. Park, "Potential applications of nanoscale semiconductor quantum devices for information and telecommunications technologies," *Mater. Sci. Eng. B*, vol. 74, nos. 1–3, pp. 1–6, May 2000, doi: 10.1016/S0921-5107(99)00524-3.

[25] A. Srivastava and M. S. Khan, "First principle study of single electron transistor based on metal-organic complex of dibenzothiophene," *Organic Electron.*, vol. 53, pp. 227–234, Feb. 2018, doi: 10.1016/j.orgel.2017.11.042.

[26] V. Khademhosseini, D. Dideban, M. T. Ahmadi, and R. Ismail, "The impact of vacancy defects on the performance of a single-electron transistor with a carbon nanotube island," *J. Comput. Electron.*, vol. 18, no. 2, pp. 428–435, Jun. 2019, doi: 10.1007/s10825-018-01290-3.

[27] A. Srivastava, B. Santhibhushan, V. Sharma, K. Kaur, M. S. Khan, M. Marathe, A. De Sarkar, and M. S. Khan, "Influence of boron substitution on conductance of Pyridine- and pentane-based molecular single electron transistors: First-principles analysis," *J. Electron. Mater.*, vol. 45, no. 4, pp. 2233–2241, Jan. 2016, doi: 10.1007/s11664-015-4287-2.

[28] S. J. Ray, "First-principles study of MoS_2, phosphorene and graphene based single electron transistor for gas sensing applications," *Sens. Actuators B, Chem.*, vol. 222, pp. 492–498, Jan. 2016, doi: 10.1016/j.snb.2015.08.039.

[29] V. K. Hosseini, M. T. Ahmadi, and R. Ismail, "Analysis and modeling of fullerene single electron transistor based on quantum dot arrays at room temperature," *J. Electron. Mater.*, vol. 47, no. 8, pp. 4799–4806, May 2018, doi: 10.1007/s11664-018-6366-7.

[30] R. K. Gupta and V. Saraf, "Nanoelectronics: Tunneling current in DNA–single electron transistor," *Current Appl. Phys.*, vol. 9, no. 1, pp. S149–S152, Jan. 2009, doi: 10.1016/j.cap.2008.03.026.

[31] A. S. Katkar, S. P. Gupta, C. Granata, C. Nappi, W. Prellier, L.-J. Chen, and P. S. Walke, "Advanced room temperature single-electron transistor of a germanium nanochain with two and multitunnel junctions," *ACS Appl. Electron. Mater.*, vol. 2, no. 7, pp. 1843–1848, Jul. 2020, doi: 10.1021/acsaelm.0c00242.

[32] V. Khademhosseini, D. Dideban, M. Ahmadi, and R. Ismail, "Current analysis of single-electron transistor based on graphene double quantum dots," *ECS J. Solid State Sci. Technol.*, vol. 9, no. 2, 2020, Art. no. 21003, doi: 10.1149/2162-8777/ab6980.

[33] Z. Wang, C. Liu, Y. Deng, Z. Huang, S. He, and D. Guo, "Carbon-based spiking neural network implemented with single-electron transistor and memristor for visual perception," in *Proc. IEEE 14th Int. Conf. Anti-Counterfeiting, Secur., Identificat. (ASID)*, Oct. 2020, pp. 143–146, doi: 10.1109/ASID50160.2020.9271721.

[34] A. Srivastava and M. S. Khan, "DFT analysis of vanadium Tris(Dithiolene)-based double-gated single-electron transistor," *J. Electron. Mater.*, vol. 49, no. 7, pp. 4203–4211, Jul. 2020, doi: 10.1007/s11664-020-08132-8.

[35] S. Parashar, "First-principles study of ultrathin single-walled nanotube-based single-electron transistor for fast-switching applications," *Phys. Solid State*, vol. 62, no. 10, pp. 1807–1814, Oct. 2020, doi: 10.1134/S1063783420100236.

[36] S. Hanurjaya, M. Anwar, M. E. Sulistyo, I. Iftadi, and S. Pramono, "Analysis of triple quantum dots single electron transistor (TQD-SET) for various configuration," *J. Electr. Electron. Inf., Commun. Technol.*, vol. 2, no. 2, pp. 56–60, doi: 10.20961/jeeict.2.2.44840.

[37] D. Biswas, A. T. Priyoti, and Q. D. M. Khosru, "Programmable single electron transistor: A modified macro-model & its applications," in *Proc. IEEE Region 10 Symp. (TENSYMP)*, Jun. 2020, pp. 1106–1109, doi: 10.1109/TENSYMP50017.2020.9230858.

[38] H. T. T. Tran, M. D. Luong, and N. H. Hoang, "Modeling of single-electron transistor in advanced design system," in *Proc. Int. Conf. Green Hum. Inf. Technol. (ICGHIT)*, Feb. 2020, pp. 62–64, doi: 10.1109/ICGHIT49656.2020.00023.

[39] M. K. Bera, "Quantum physics-based analytical modeling of drain current of single electron transistor with island made of zigzag-tungsten disulfide nanoribbon," *East Eur. J. Phys.*, vol. 19, no. 4, pp. 21–27, Nov. 2020, doi: 10.26565/2312-4334-2020-4-03.

[40] S. Chauhan and A. S. Verma, "First-principles calculations of carbon-nanotube and boron-nanotube based single-electron transistors," *East Eur. J. Phys.*, vol. 1, pp. 66–74, Feb. 2020, doi: 10.26565/2312-4334-2020-1-05.

[41] R. Parekh, "Design and simulation of single-electron transistor-based SRAM and its memory controller at room temperature," *Int. J. Integr. Eng.*, vol. 11, no. 6, pp. 186–195, 2019. [Online]. Available: https://publisher.uthm.edu.my/ojs/index.php/ijie/article/view/2955

[42] M. Abdelkrim, "Modeling and simulation of single-electron transistor (SET) with aluminum island using neural network," *Carpathian J. Electron. Comput. Eng.*, vol. 12, no. 1, pp. 23–28, Sep. 2019, doi: 10.2478/cjece-2019-0005.

[43] R. Patel, Y. Agrawal, and R. Parekh, "Design of prominent SET-based high performance computing system," *IET Circuits, Devices Syst.*, vol. 14, no. 2, pp. 159–167, Mar. 2020, doi: 10.1049/iet-cds.2019.0166.

[44] V. Khademhosseini, D. Dideban, M. Ahmadi, R. Ismail, and H. Heidari, "Investigating the electrical characteristics of a single electron transistor utilizing graphene nanoribbon as the island," *J. Mater. Sci., Mater. Electron.*, vol. 30, no. 8, pp. 8007–8013, Apr. 2019, doi: 10.1007/s10854-019-01121-6.

[45] S. J. Lee, J. Kim, T. Tsuda, R. Takano, R. Shintani, K. Nozaki, and Y. Majima, "Single-molecule single-electron transistor (SM-SET) based on π-conjugated quinoidal-fused oligosilole and heteroepitaxial spherical Au/Pt nanogap electrodes," *Appl. Phys. Exp.*, vol. 12, no. 12, Dec. 2019, Art. no. 125007, doi: 10.7567/1882-0786/ab56e5.

[46] M. Z. Ahsan, "Single-electron transistor (SET): Operation and application perspectives," *MIST Int. J. Sci. Technol.*, vol. 6, no. 1, pp. 1–5, 2018.

[47] V. KhademHosseini, D. Dideban, M. T. Ahmadi, and R. Ismail, "An analytical approach to model capacitance and resistance of capped carbon nanotube single electron transistor," *AEU Int. J. Electron. Commun.*, vol. 90, pp. 97–102, Jun. 2018, doi: 10.1016/j.aeue.2018.04.015.

[48] F. Castro, I. Savidis, and A. Sarmiento, "A quasi-analytic behavioral model for the single-electron transistor for hybrid MOS/SET circuit simulation," in *Proc. IEEE 13th Nanotechnol. Mater. Devices Conf. (NMDC)*, Oct. 2018, pp. 1–4, doi: 10.1109/NMDC.2018.8605730.

[49] M. Miralaie and A. Mir, "Evaluation of room-temperature performance of ultra-small single-electron transistor-based analog-to-digital convertors," *J. Circuits, Syst. Comput.*, vol. 27, no. 14, Dec. 2018, Art. no. 1850217, doi: 10.1142/S0218126618502171.

[50] S. Barraud, I. Duchemin, L. Hutin, Y. Niquet, and M. Vinet, "Single-electron transistor and its fabrication method," U.S. Patent 9 911 841, Mar. 6, 2018.

[51] Z. Bai, X. Liu, Z. Lian, K. Zhang, G. Wang, S.-F. Shi, X. Pi, and F. Song, "A silicon cluster based single electron transistor with potential room-temperature switching," *Chin. Phys. Lett.*, vol. 35, no. 3, Mar. 2018, Art. no. 037301, doi: 10.1088/0256-307X/35/3/037301.

[52] R. Patel, Y. Agrawal, and R. Parekh, "A vector file generation program for simulating single electron transistor based computing system," in *Proc. IEEE Electron Devices Kolkata Conf. (EDKCON)*, Nov. 2018, pp. 647–650, doi: 10.1109/EDKCON.2018.8770464.

[53] T. S. Delwar, S. Biswas, and A. Jana, "Realization of hybrid single electron transistor based low power circuits in 22 nm technology," *Comput. Sci. Eng.*, no. 27, 2017. [Online]. Available: https://www.researchgate.net/publication/319164922_Realization_hybrid_single_electron_transistor_based_low_power_circuits_in_nm_technology, doi: 10.1201/9781315375021-7.
[54] E. Amat, J. Bausells, and F. Perez-Murano, "Exploring the influence of variability on single-electron transistors into SET-based circuits," *IEEE Trans. Electron. Devices*, vol. 64, no. 12, pp. 5172–5180, Dec. 2017, doi: 10.1109/TED.2017.2765003.
[55] A. Ghosh, A. Jain, N. B. Singh, and S. K. Sarkar, "A modified macro model approach for SPICE based simulation of single electron transistor," *J. Comput. Electron.*, vol. 15, no. 2, pp. 400–406, Jun. 2016, doi: 10.1007/s10825-015-0790-1.
[56] F. Willy and Y. Darma, "Modeling and simulation of single electron transistor with master equation approach," *J. Phys., Conf. Ser.*, vol. 739, Aug. 2016, Art. no. 012048, doi: 10.1088/1742-6596/739/1/012048.
[57] V. Raut and P. Dakhole, "Design and implementation of quaternary summation circuit with single electron transistor and MOSFET," in *Proc. Int. Conf. Electr., Electron., Optim. Techn. (ICEEOT)*, Mar. 2016, pp. 2226–2229, doi: 10.1109/ICEEOT.2016.7755088.
[58] M. Miralaie and A. Mir, "Performance analysis of single-electron transistor at room-temperature for periodic symmetric functions operation," *J. Eng.*, vol. 2016, no. 10, pp. 352–356, Oct. 2016, doi: 10.1049/joe.2016.0139.
[59] A. Jain, A. Ghosh, N. B. Singh, and S. K. Sarkar, "A new SPICE macro model of single electron transistor for efficient simulation of single-electronics circuits," *Anal. Integr. Circuits Signal Process.*, vol. 82, no. 3, pp. 653–662, Mar. 2015, doi: 10.1007/s10470-015-0491-5.
[60] S. Mukherjee, A. Jana, and S. K. Sarkar, "Hybrid single electron transistor-based low power consuming BCD adder circuit in 65 nanometer technology," in *Computational Advancement in Communication Circuits and Systems*. New Delhi, India: Springer, 2015, pp. 375–381, doi: 10.1007/978-81-322-2274-3_41.
[61] V. Raut and P. K. Dakhole, "Design and implementation of four bit arithmetic and logic unit using hybrid single electron transistor and MOSFET at 120nm technology," in *Proc. Int. Conf. Pervas. Comput. (ICPC)*, Jan. 2015, pp. 1–6, doi: 10.1109/PERVASIVE.2015.7087063.
[62] G. Karbasian, A. O. Orlov, and G. L. Snider, "Fabrication of nanodamascene metallic single-electron transistors with atomic layer deposition of tunnel barrier," *J. Vac. Sci. Technol. B, Nanotechnol. Microelectron. Mater. Process. Meas. Phenom.*, vol. 33, no. 6, 2015, Art. no. 06FG02, doi: 10.1116/1.4932156.
[63] L.-N. Su, L. Lv, X.-X. Li, H. Qin, and X.-F. Gu, "Fabrication and characterization of a single electron transistor based on a silicon-on-insulator," *Chin. Phys. Lett.*, vol. 32, no. 4, Apr. 2015, Art. no. 047301, doi: 10.1088/0256-307X/32/4/047301.
[64] F. Soto, J. Wang, R. Ahmed, and U. Demirci, "Medical Micro/Nanorobots in precision medicine," *Adv. Sci.*, vol. 7, no. 21, Nov. 2020, Art. no. 2002203, doi: 10.1002/advs.202002203.
[65] J. Li, B. Esteban-Fernández de Ávila, W. Gao, L. Zhang, and J. Wang, "Micro/nanorobots for biomedicine: Delivery, surgery, sensing, and detoxification," *Sci. Robot.*, vol. 2, no. 4, Mar. 2017, Art. no. eaam6431, doi: 10.1126/scirobotics.aam6431.
[66] Z. Wu, Y. Chen, D. Mukasa, O. S. Pak, and W. Gao, "Medical micro/nanorobots in complex media," *Chem. Soc. Rev.*, vol. 49, no. 22, pp. 8088–8112, Nov. 2020, doi: 10.1039/D0CS00309C.
[67] A. V. Singh, M. H. D. Ansari, P. Laux, and A. Luch, "Micro-nanorobots: Important considerations when developing novel drug delivery platforms," *Expert Opinion Drug Del.*, vol. 16, no. 11, pp. 1259–1275, Nov. 2019, doi: 10.1080/17425247.2019.1676228.
[68] X.-Z. Chen, M. Hoop, F. Mushtaq, E. Siringil, C. Hu, B. J. Nelson, and S. Pané, "Recent developments in magnetically driven micro- and nanorobots," *Appl. Mater. Today*, vol. 9, pp. 37–48, Dec. 2017, doi: 10.1016/j.apmt.2017.04.006.
[69] M. Luo, Y. Feng, T. Wang, and J. Guan, "Micro-/nanorobots at work in active drug delivery," *Adv. Funct. Mater.*, vol. 28, no. 25, Jun. 2018, Art. no. 1706100, doi: 10.1002/adfm.201706100.
[70] S. Dolev, R. P. Narayanan, and M. Rosenblit, "Design of nanorobots for exposing cancer cells," *Nanotechnology*, vol. 30, no. 31, Aug. 2019, Art. no. 315501, doi: 10.1088/1361-6528/ab1770.
[71] M. Wang, Y. Wang, Z. Yang, T. Chen, L. Sun, and T. Fukuda, "Cooperation method of symmetrically distributed multi-nanorobotic manipulators inside SEM for nanodevice constructing," in *Proc. IEEE 13th Annu. Int. Conf. Nano/Micro Eng. Mol. Syst. (NEMS)*, Apr. 2018, pp. 543–548, doi: 10.1109/NEMS.2018.8556984.
[72] F. Xue, L. Chen, L. Wang, Y. Pang, J. Chen, C. Zhang, and Z. L. Wang, "MoS_2 tribotronic transistor for smart tactile switch," *Adv. Funct. Mater.*, vol. 26, no. 13, pp. 2104–2109, Apr. 2016, doi: 10.1002/adfm.201504485.
[73] N. Xin, J. Guan, C. Zhou, X. Chen, C. Gu, Y. Li, M. A. Ratner, A. Nitzan, J. F. Stoddart, and X. Guo, "Concepts in the design and engineering of single-molecule electronic devices," *Nature Rev. Phys.*, vol. 1, no. 3, pp. 211–230, Feb. 2019, doi: 10.1038/s42254-019-0022-x.
[74] K. Kornobis, N. Kumar, P. Lodowski, M. Jaworska, P. Piecuch, J. J. Lutz, B. M. Wong, and P. M. Kozlowski, "Electronic structure of the S1 state in methylcobalamin: Insight from CASSCF/MC-XQDPT2, EOM-CCSD, and TD-DFT calculations," *J. Comput. Chem.*, vol. 34, no. 12, pp. 987–1004, May 2013, doi: 10.1002/jcc.23204.
[75] K. Kornobis, N. Kumar, B. M. Wong, P. Lodowski, M. Jaworska, T. Andruniów, K. Ruud, and P. M. Kozlowski, "Electronically excited states of vitamin B_{12}: Benchmark calculations including time-dependent density functional theory and correlated ab initio methods," *J. Phys. Chem. A*, vol. 115, no. 7, pp. 1280–1292, Feb. 2011, doi: 10.1021/jp110914y.
[76] D. Dey, P. Roy, and D. De, "Electronic transport properties of electrically doped cytosine-based optical molecular switch with single-wall carbon nanotube electrodes," *IET Nanobiotechnol.*, vol. 13, no. 5, pp. 484–492, Jul. 2019, doi: 10.1049/iet-nbt.2018.5375.
[77] M. Schwarze, K. S. Schellhammer, K. Ortstein, J. Benduhn, C. Gaul, A. Hinderhofer, L. Perdigón Toro, R. Scholz, J. Kublitski, S. Roland, M. Lau, C. Poelking, D. Andrienko, G. Cuniberti, F. Schreiber, D. Neher, K. Vandewal, F. Ortmann, and K. Leo, "Impact of molecular quadrupole moments on the energy levels at organic heterojunctions," *Nature Commun.*, vol. 10, no. 1, pp. 1–9, Jun. 2019, doi: 10.1038/s41467-019-10435-2.
[78] P. K. Nayak and N. Periasamy, "Calculation of electron affinity, ionization potential, transport gap, optical band gap and exciton binding energy of organic solids using 'solvation' model and DFT," *Organic Electron.*, vol. 10, no. 7, pp. 1396–1400, Nov. 2009, doi: 10.1016/j.orgel.2009.06.011.
[79] R. Ismail, M. T. Ahmadi, and S. Anwar, *Advanced nanoelectronics*. Boca Raton, FL, USA: CRC Press, 2018.
[80] M. H. Rashid, A. Koel, T. Rang, and M. H. Ziko, "Simulations of benzene and hydrogen-sulfide gas detector based on single-walled carbon nanotube over intrinsic 4H-SiC substrate," *Micromachines*, vol. 11, no. 5, p. 453, Apr. 2020, doi: 10.3390/mi11050453.

MORTEZA BODAGHZADEH received the B.Sc. degree in physics from the University of Tabriz, Iran, in 2015, and the M.Sc. degree in nanotechnology sciences–nanophysics from Urmia University, Iran, in 2018. Since 2016, he has been working as a Researcher at the Nano-Sensor Research Group, and a Research Assistant and a Laboratory Assistant with the Nanotechnology Research Center, Urmia University, and a Laboratory Assistant, a Researcher, and a Technician with Urmia Mahan Nanotechnology Company (UMNT). His research interests include simulation, modeling, designing, and improving the performance of nanotechnology devices, nano-materials, NEMS, and nano-electronic systems, in particular the new generation of carbon nanotube/graphene-based transistors, TFETs, molecular/single-electron transistors, nano/bio sensors, and nano-devices compatible with the human body for drug delivery and destruction of tumors and cancer cells.

MOHAMAD TAGHI AHMADI received the Ph.D. degree in electrical engineering from Makmal nano Universiti Teknologi Malaysia on graphene-based nanoelectronic devices. He has completed the postdoctoral research at Makmal nano Universiti Teknologi Malaysia. He was the Former Deputy Dean (research) at the Faculty of Nanotechnology, Urmia University, a Visiting Associate Professor at Malaysia-Japan Institute of Technology (MJIIT) and Universiti Teknologi Malaysia (UTM), an Invited Senior Researcher at Universiti Teknologi Malaysia, and an Assistant Professor of electrical engineering at UTM. He is currently an Associate Professor with the Department of Nano-Physics, Urmia University, Urmia, Iran. His research interests include nanoscale non-classical device (sensors and transistors) simulation, modeling, and characterization. He was awarded the Universiti Teknologi Malaysia (UTM) Chancellor Award, the UTM Best Publication Award (CITRA KARISMA 2013), the UTM Academic Excellence Award, the UTM Postdoctoral Fellowship Award, and the Best Ph.D. Student Award (International Student Center Iranian Student Society).

MAHAN AHMADI is currently a Medical Researcher with Xi'an Jiaotong University (XJTU), Xi'an, China, who has been nominated as one of the outstanding students at XJTU, for consecutive years 2018–2021. He is one of the founding members of the International Student Ambassadors (ISA) at XJTU (medical campus).

SEYED SAEID RAHIMIAN KOLOOR received the M.Sc. and Ph.D. degrees (Hons.) in the field of applied mechanics and design from the Universiti Teknologi Malaysia (UTM), from 2008 to 2015. He had been working as the Project Manager and three times as a Postdoctoral Researcher at UTM, Iran University of Science and Technology (IUST), and Iran's National Elites Foundation (BMN). He is currently a Senior Scientist with the Institute for Nanomaterials, Advanced Technologies, and Innovation (CXI), Technical University of Liberec (TUL), Liberec, Czech Republic. He has authored many articles that are published and presented in international journals and conferences. His research interests include characterization, modeling, simulation, and experimentation of materials and structures at different scales. He is serving as a member for the Elsevier Advisory Panel, the editorial board, and a guest editor for many international journals, and served as a committee member for many international conferences.

MICHAL PETRŮ is currently an Associate Professor in design and machine parts with the Faculty of Mechanical Engineering, Technical University of Liberec (TUL), Liberec, Czech Republic. He is also the Head of the Department of Machinery Construction, Institute for Nanomaterials, Advanced Technology, and Innovation (CXI), TUL. He has authored many scientific and industrial research articles that are published in the area of numerical modeling and optimum design of the machine (more than 50 papers in SCOPUS and ISI WOS databases), and 20 patents and utility samples. His research interests include nanoscale characterization and simulation of materials and structures.

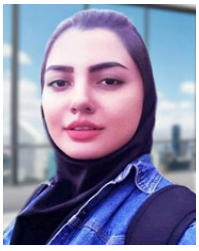

FATEMEH ESFANDIARI received the B.Sc. degree in psychology from Shiraz University, Iran, in 2019, and the M.Sc. degree in clinical psychology from Shahid Chamran University, Iran, in 2021. She is currently a Researcher with the College of Education and Psychology, Shahid Chamran University. Her research interests include neurodegenerative diseases, cognitive neuroscience, and artificial intelligence.